ACS APPLIED POLYMER MATERIALS

Article

Cite This: ACS Appl. Polym. Mater. 2019, 1, 3313−3322

pubs.acs.org/acsapm

Effect of Cyano Substitution on Conjugated Polymers for Bulk Heterojunction Solar Cells

Qianqian Zhang,[†] Jeromy James Rech,[†] Liang Yan,[†] Quanbin Liang,[§] Zhengxing Peng,[‡] Harald Ade,[‡] Hongbin Wu,[§] and Wei You[†,*]

[†]Department of Chemistry, University of North Carolina at Chapel Hill, Chapel Hill, North Carolina 27599, United States

[‡]Department of Physics and Organic and Carbon Electronics Lab (ORaCEL), North Carolina State University, Raleigh, North Carolina 27695, United States

[§]Institute of Polymer Optoelectronic Materials and Devices, State Key Laboratory of Luminescent Materials and Devices, South China University of Technology, Guangzhou 510640, P. R. China

Supporting Information

ABSTRACT: The design of polymer structures has played a vital role in improving the efficiency of organic solar cells (OSCs). A common approach to increase solar cell efficiency is to add a specific substituent to the polymer backbone; yet, the cyano substituent, a strong electron-withdrawing group, has not received much attention as such substituents with conjugated polymers. In this study, we systematically explore the impact of cyano substitution on conjugated polymers by varying the amount of cyano groups, from zero to two per repeat unit, on the benzotriazole acceptor moiety of our polymers. We find that cyano substitution effectively decreases the energy levels of the polymer, leading to high V_{OC} values; however, the impact of additional cyano groups offer diminishing returns. Moreover, cyano substitution also decreases the band gap of the polymers, inducing a shift of polymer absorption to longer wavelength. Along with the optical and electrochemical differences, the cyano effect was also thoroughly characterized by changes in morphology, charge transfer state energy, charge carrier density, lifetime, and nongeminate recombination rate. The champion polymer (efficiency of 8.6%) has a single cyano substituent, monoCNTAZ, which affords high V_{OC}, J_{SC}, and FF due to deep energy level, red-shifted absorption, and efficient charge transport properties, respectively. However, further additions of cyano groups degrade the performance. Overall, this work highlights the benefits and limitations of cyano functionalization on conjugated polymers for OSCs.

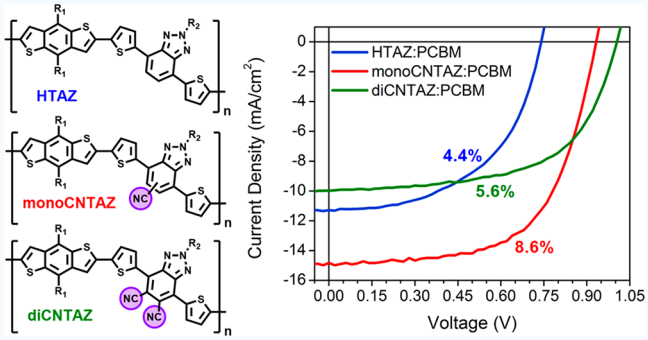

KEYWORDS: *organic photovoltaic, organic solar cells, polymer solar cells, conjugated polymers, cyano substitution, structure−property relationship*

1. INTRODUCTION

Organic solar cells (OSCs) can offer many unique properties that are unavailable with other forms of solar cell technology, such as solution processability, low cost, semitransparency, flexibility, and are lightweight.[1−5] Because of these advantages, it is important to work on developing high-performance materials (polymers and small molecules) that can be used in OSCs. For conjugated polymers, methods to boost the efficiency include adjusting the polymer backbone, developing new donor and acceptor moieties, tuning side chains, and incorporating substituents.[6−12] Among those strategies, incorporating proper substituents on high-performance polymers is of special interest to further improve the properties of polymers without modifying the essential backbones of polymers.

The most widely studied electron-withdrawing substituent is fluorine, which can effectively tune the energy levels, charge transport properties, and morphology of the active layer of OSCs and correspondingly improve the efficiency of OSCs.[13−15] However, some limitations are associated with fluorine substitution: due to the resonance-donating properties of fluorine, the decrease of the energy levels of polymers induced by fluorine substitution is limited, which consequently limits the enhancement of the open-circuit voltage (V_{OC}); moreover, the effect of fluorine on the band gap and absorption of conjugated polymers is usually minor, which hinders the improvement of the short circuit current density (J_{SC}) by absorption of fluorinated polymers.[13−15] To provide an example, we recently found that putting fluorine substituents on appropriate positions of thiophene linker

Received: August 16, 2019
Accepted: October 28, 2019
Published: October 29, 2019

DOI: 10.1021/acsapm.9b00767
ACS Appl. Polym. Mater. 2019, 1, 3313−3322

units can extend the absorption of polymers by planarizing the polymer backbones;[16] however, the red-shift induced by fluorinating thiophene units only occurred when substituted to certain locations. As a result, J_{SC} values of corresponding devices were only marginally improved.

Compared to the widely studied fluorine substitution, the cyano functional group is a stronger electron-withdrawing functional group due to the inductive and resonance effects; thus, adding the cyano substituent to conjugated polymer backbones can decrease the highest occupied molecular orbital (HOMO) energy level of the polymer by a larger degree and shift the absorption of the polymers to a longer wavelength, which benefits the V_{OC} and J_{SC} of the solar cells, respectively.[17,18] Currently, cyano units are widely used in nonfullerene acceptors end groups; however, cyano-substituted polymers with high performance have not been widely reported.[19−23] In our previous study, Li et al. developed a benzotriazole (TAZ)-acceptor-moiety-based polymer with two cyano units on the TAZ unit (CNTAZ, renamed diCNTAZ herein for clarity)[21] and achieved an efficiency of 6.0%. While a high V_{OC} was obtained with a deeply lying HOMO level, the J_{SC} was low despite the large red-shift of absorption, which, together with the low fill factor (FF), limited the improvement of efficiency to a higher value. However, by adding a single cyano unit to a pyridine-fused-triazole (PyTAZ) unit (PyCNTAZ), Li et al. were able to achieve a high efficiency of 8.4% with phenyl-C_{61}-butyric acid methyl ester (PCBM) as the electron acceptor material with much improved V_{OC}, J_{SC}, and FF. While this result shows great promise, the source of the distinct device performance of diCNTAZ and PyCNTAZ was unclear because of the structural differences: which of the different chemical structures (PyTAZ unit vs TAZ unit) or the amount of cyano units (one vs two per repeating unit) played the most important role?

In order to get a comprehensive understanding of the effect of the cyano substitution on polymers, in this study, we synthesized a series of polymers with varying amounts of cyano groups on the TAZ unit: HTAZ (0), monoCNTAZ[17] (1), and diCNTAZ (2). Along with understanding the optical, electrochemical, and photovoltaic characteristics, we also explored changes in morphology, charge transfer state energy, charge carrier density and lifetime, and nongeminate recombination rate as the number of cyano substituents changes. Interestingly, the monoCNTAZ polymer outperformed both the HTAZ and diCNTAZ when these polymers were employed in OSCs. With just one cyano substituent per repeating unit, monoCNTAZ blends achieved a high V_{OC} value close to that of diCNTAZ. In addition, the red-shifted absorption of monoCNTAZ effectively resulted in a high J_{SC} of its solar cells. Also, the noticeably improved hole mobility of monoCNTAZ blends improved the FF; thus, a high efficiency of 8.6% (average) was achieved by monoCNTAZ:PCBM blends. Our results demonstrate both the benefits that cyano functionalization can offer and the limitations of this approach.

2. RESULTS AND DISCUSSION

2.1. Synthesis. The conjugated polymers were made via step growth polymerization between the benzodithiophene monomer (*m*-BnDT) and functionalized benzotriazole monomer (*m*-TAZ), as shown in Scheme 1. For clarity, we will use HTAZ, monoCNTAZ, and diCNTAZ to represent the polymers and use *m*-HTAZ, *m*-monoCNTAZ, and *m*-diCNTAZ to represent the corresponding *m*-TAZ-based monomers in the following discussion.

The synthesis of *m*-BnDT and *m*-HTAZ follows literature procedures,[16,24] and the reaction schemes for *m*-monoCNTAZ and *m*-diCNTAZ are shown in Scheme 2. The starting material for the *m*-monoCNTAZ is 3,4-diaminobenzonitrile (compound **1**). Compound **1** underwent oxidative bromination with potassium bromide, hydrogen bromide acid, and *tert*-butyl hydroperoxide to achieve compound **2**.[25] Following purification, compound **2** was cyclized to obtain the triazole structure of compound **3**. After alkylation of the N-2 position of compound **3**, compound **4** was then subjected to the Stille coupling reaction with a stannylated thiophene linker to achieve compound **5**. Afterward, compound **5** was subsequently brominated by excessive *N*-bromosuccinimide (NBS) to obtain the *m*-monoCNTAZ. Please note that the substitution of one CN group on the TAZ unit significantly reduces the reactivity of compound **5**, so excessive NBS together with an extended time (7 days) was needed. Even through these reaction conditions are unfavorable, the resulting monomer was made with appropriate yields and after recrystallization had very high purity appropriate for polymerization. Reaction details are included in the Supporting Information (SI).

We have previously reported the synthesis of *m*-diCNTAZ based on a general methodology, which is shown as Pathway A in Scheme S1.[21] In this study, a new synthetic approach, Pathway B (Scheme S1), was developed to get *m*-diCNTAZ from fluorinated TAZ monomer (*m*-FTAZ) via nucleophilic aromatic cyanation (shown in Scheme 2), as *m*-FTAZ can be readily prepared with higher yields. After we succeeded to prepare *m*-diCNTAZ through the new reaction approach, Casey et al. reported a similar synthetic approach through nucleophilic aromatic cyanation on an FTAZ compound but without the bromo unit.[23] They also brominated the cyano-substituted TAZ compound to obtain the final monomer, which thus also suffered from the low yield in the bromination step due to the decreased reactivity with the strong electron-withdrawing cyano unit.[23] Comparing the two different pathways (Scheme S1), each has the same number of reaction steps, and the yields for most steps are similar, with the key exception of the last two steps. In Pathway A, the condensation of compound **12** and succinonitrile suffers from a low yield of 37%. This is nearly half the yield of the new approach (Pathway B) to add the cyano substituents (60%). Also in Pathway A, NBS was unable to brominate the monomer because of the highly electron deficient backbone. Instead of NBS, molecular bromine was required to make the final monomers. Along with lower yields, molecular bromine can more easily lead to overbromination. Using the new approach of Pathway B, the bromination of the fluorinated benzotriazole can be done in higher yields with the milder NBS reagent. Therefore, when comparing the overall yields of both synthetic approaches, the newly developed Pathway B offers a higher overall yield of 7.2%, which is 2.5× higher than the 2.8% yield from the originally reported Pathway A. This new pathway is also advantageous, as many current fluorinated monomers can be converted to cyano functionalized polymers in a single reaction, allowing for many new types of conjugated polymers to be made.

Finally, the polymers (HTAZ, monoCNTAZ, and diCNTAZ) were synthesized through microwave-assisted Stille-coupling-based polymerization methodology.[26] The number

DOI: 10.1021/acsapm.9b00767
ACS Appl. Polym. Mater. 2019, 1, 3313−3322

Scheme 1. Microwave-Assisted Stille-Polycondensation Approach to the Synthesis of Three Polymers: HTAZ, monoCNTAZ, and diCNTAZ[a]

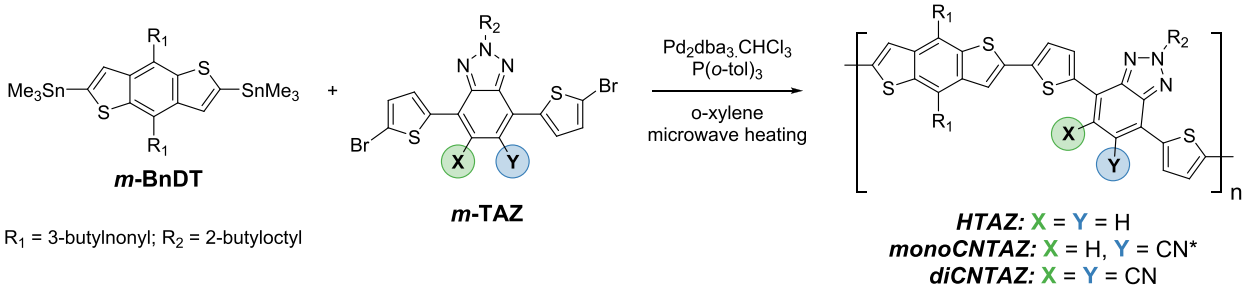

[a]The cyano group of monoCNTAZ can be in either the X or Y position, so both X = H, Y = CN and X = CN, Y = H represent the monoCNTAZ polymer.

Scheme 2. Synthesis of monoCNTAZ and diCNTAZ Monomers

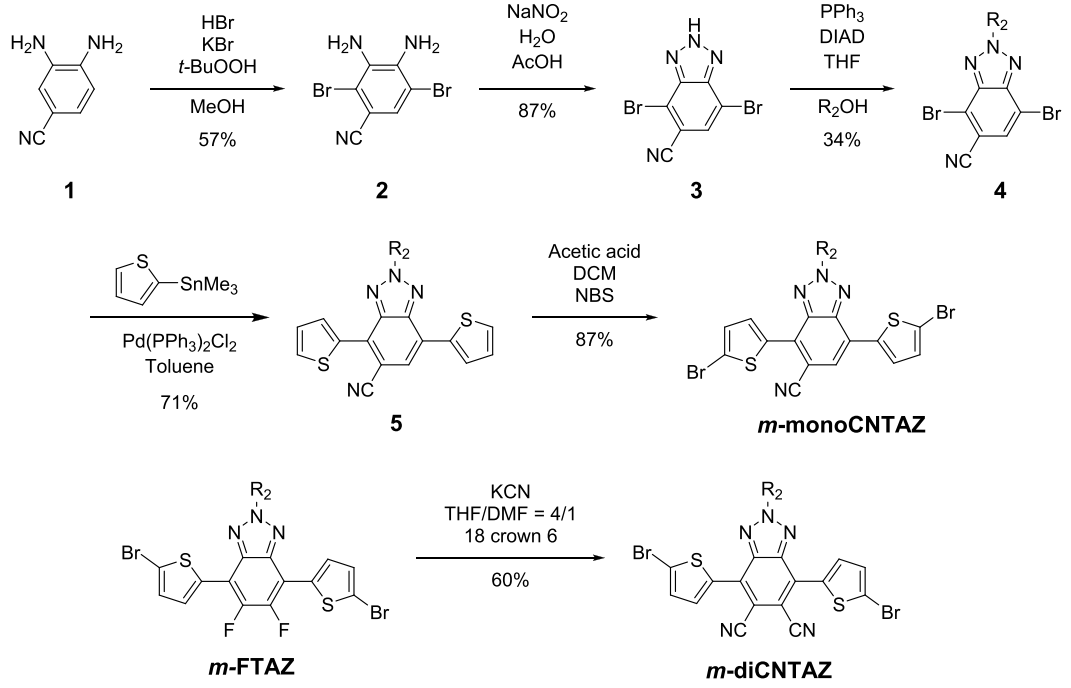

average molar mass (M_n) of each polymer, ranging from 44 to 52 kg/mol, was optimized by adjusting the monomer ratios. The molar mass for each polymer was measured through high-temperature gel permeation chromatography (HT-GPC), and the resulting traces are shown in Figure S1. The polymers all exhibited high thermal stability, with a decomposition temperature (T_d, 5% weight loss temperature) around 400 °C, as measured by thermogravimetric analysis (TGA) and no thermal transitions in the processing window, as measured by differential scanning calorimetry (DSC) (Figure S2). All three polymers can be dissolved in common solvent used in OSCs, such as chloroform and chlorobenzene at elevated temperature. While the solubility of monoCNTAZ is significantly reduced when compared to HTAZ and diCNTAZ, it is still appropriate for device fabrication. More synthetic details about the synthesis of the polymers were included in the SI.

2.2. Optical and Electrochemical Properties. Once the polymers were synthesized, the first characterization approach was to look at the optical and electrochemical properties for each. To begin with, the optical properties of the polymers were investigated with UV−vis absorption of the polymer solution in 1,2-dichlorobenzene (*o*-DCB) (Figure 1a) and polymer thin films (Figure 1b). By comparison, a gradual bathochromic shift of the UV−vis absorption induced by cyano substituents was observed: for each cyano substituent, the absorption edge shows a red-shift by 30−40 nm, and the optical band gap decreases by ∼0.1 eV. Additionally, the UV−vis absorption spectra of the polymers in solution at room temperature are almost the same with those of thin films, which means the polymer chains already aggregate in the solution at ambient conditions. Finally, the thickness-normalized absorption coefficient is both high (∼10^5 cm^{-1}) and similar for each of the polymers, suggesting the key impact of the cyano substituent is the red-shift of absorbance.

Next, the electrochemical properties of each polymer were measured through cyclic voltammetry (CV). The HOMO energy levels of the polymers were measured by the onset of the oxidation peaks, shown in Figure 1c. Using the ferrocene/ferrocenium reference peak, the HOMO levels are estimated to be −5.48, −5.58, and −5.60 eV for HTAZ, monoCNTZ, and diCNTAZ, respectively (more details available in the SI). This follows as the strong electron-withdrawing nature of the cyano

DOI: 10.1021/acsapm.9b00767
ACS Appl. Polym. Mater. 2019, 1, 3313−3322

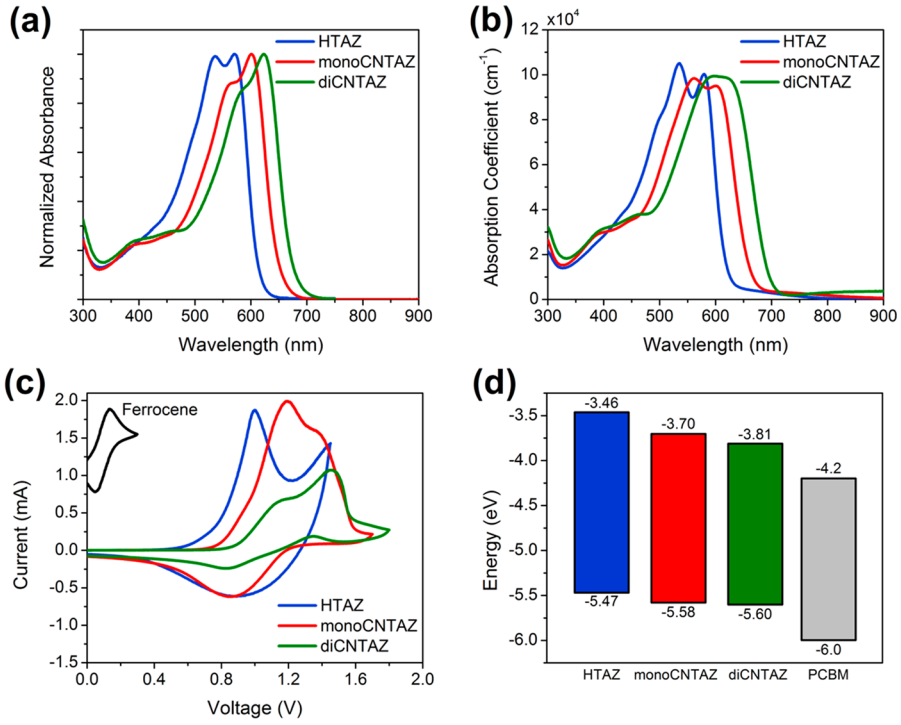

Figure 1. (a) Solution UV−vis for HTAZ, monoCNTAZ, and diCNTAZ in 1,2-dichlorobenzene, (b) thickness-normalized absorption coefficient of thin polymer films measured through UV−vis, (c) cyclic voltammetry of polymer thin films to determine HOMO energy level using a three-electrode setup of a glassy carbon working electrode, Ag/Ag^+ reference electrode, and Pt counter electrode, and (d) resulting HOMO/LUMO energy level diagram for each polymer and PCBM in this study.

Table 1. Molar Mass, Optical, and Electrochemical Properties of the Three Polymers

polymer	M_n (kg/mol)	$Đ$ (M_w/M_n)	absorbance onset (nm)	HOMO[a] (eV)	LUMO[b] (ev)	optical band gap[c] (eV)
HTAZ	44.1	3.0	616	−5.47	−3.46	2.01
monoCNTAZ	52.0	3.5	658	−5.58	−3.70	1.88
diCNTAZ	50.6	3.3	693	−5.60	−3.81	1.79

[a]HOMO levels were estimated by cyclic voltammetry. [b]LUMO = HOMO + optical band gap. [c]Optical band gap was estimated from the onset of absorption of polymer films.

substituent should pull down the energy levels of the conjugated polymer. Interestingly, the degree of the HOMO level decrease induced by the second cyano unit is smaller than that induced by the first cyano unit, indicating that further addition of the cyano substituent to already electron-deficient aromatics only offers a diminished return. Similar behavior has been observed in our previous report, where the PBnDT-FTAZ polymer (with difluorinated benzotriazole) only has a negligible decrease of the HOMO energy level when compared with the HOMO of the monofluorinated version.[27] The energy levels for each polymer and PCBM are shown in Figure 1d. The lowest occupied molecular orbital (LUMO) energy level is estimated through using the HOMO energy level found via CV and the optical band gap measured from the absorption onset of the UV−vis spectra. A summary of the optical and electrochemical properties can be found in Table 1.

2.3. Photovoltaic Properties. The photovoltaic properties of the three polymers were investigated in the bulk heterojunction (BHJ) solar cells with a conventional device configuration: indium doped tin oxide (ITO)/copper(I) thiocyanate (CuSCN)/polymer:PCBM/Ca/Al. The weight ratio of the polymer:PCBM was 1:2 for all the three polymer blends, and because of the deep HOMO energy levels of the polymers, CuSCN was selected as the hole transporting layer.[28] The $J-V$ curves and EQE curves of thick (∼300 nm) solar cell devices are presented in Figure 2, separately, with the related device characteristics summarized in Table 2. The photovoltaic properties of the solar cell devices at different thicknesses can be found in Table S2, and slightly higher efficiency can be obtained at a lower thickness for HTAZ and diCNTAZ. In addition to the above device architecture, a second set of devices were fabricated with a slightly modified structure of ITO/PEDOT:PSS/polymer:PCBM/PFN (5 nm)/Al (80 nm), where PFN is poly[(9,9-bis(3′-(*N*,*N*-dimethylamino)propyl)-2,7-fluorene)-*alt*-2,7-(9,9−dioctyl-fluorene)].[29] This device structure was used for transient photocurrent (TPC) and transient photovoltage (TPV) measurements (vide infra). The efficiencies of the devices used for TPC and TPV are also shown in Table 2. Both device architectures produce similar photovoltaic characteristics. We note that the devices with the PFN interlayer show a relatively higher FF regardless of the active layer, indicating that PFN plays an role in facilitating charge transport and extraction.[30] On the other side, the J_{SC} values of corresponding devices with the PFN interlayer were smaller, which can be ascribed to the (a) unfavorable nanoscale morphology of the active layer when PFN was used and (b) thinner films of the devices with the PFN interlayer. Nevertheless, these devices show similar trends

DOI: 10.1021/acsapm.9b00767
ACS Appl. Polym. Mater. 2019, 1, 3313−3322

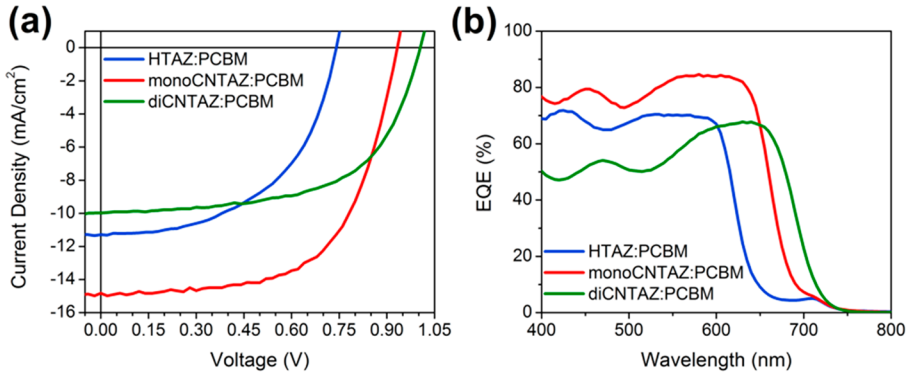

Figure 2. (a) Representative $J-V$ and (b) EQE curves of each OSC device.

Table 2. Photovoltaic Properties of the Various Polymer Solar Cells

polymer	stack[a]	thickness (nm)	J_{SC} (mA/cm^2)	V_{OC} (V)	FF (%)	PCE (%)
HTAZ	A	249	11.10 ± 0.25	0.741 ± 0.001	53.3 ± 1.3	4.39 ± 0.17
	B	153	10.11 ± 0.17	0.757 ± 0.002	58.5 ± 1.8	4.48 ± 0.19
monoCNTAZ	A	333	14.97 ± 0.40	0.932 ± 0.001	61.6 ± 1.1	8.60 ± 0.27
	B	270	13.28 ± 0.28	0.921 ± 0.003	62.8 ± 1.3	7.68 ± 0.29
diCNTAZ	A	282	11.30 ± 0.33	0.998 ± 0.008	49.6 ± 1.5	5.59 ± 0.28
	B	112	8.81 ± 0.44	1.043 ± 0.002	63.6 ± 0.9	5.85 ± 0.26

[a]There are two different device architectures used: A = ITO/CuSCN/polymer:PCBM/Ca/Al and B = ITO/PEDOT:PSS/polymer:PCBM/PFN/Al.

in V_{OC} and J_{SC}, thus enabling us to probe charge carrier recombination dynamics in freshly made devices.

In terms of the impact of the cyano groups on photovoltaic properties, the first clear trend is with the V_{OC}. Much like the HOMO energy level differences, cyano functionalization increased the V_{OC}, but the addition of the second cyano had diminished returns. With the second device architecture (where PFN was used as the interlayer), the FF also increases with cyano content; however, the large decrease in J_{SC} erodes the values of this FF increase. Out of the three polymers, the highest average efficiency of 8.6% is achieved by monoCNTAZ:PCBM, nearly double that of HTAZ:PCBM-based devices with 4.4%. For diCNTAZ:PCBM, with the addition of the second cyano group, a significant drop of J_{SC} leads to a significant decrease in PCE to 5.6%. While cyano substitution effectively red-shifts the absorption of the polymer, as shown in Figure 2b, EQE values of diCNTAZ-based devices are significantly lower than HTAZ. In contrast, the EQE values of monoCNTAZ-based devices are higher over the whole absorption range than HTAZ and diCTAZ, as is the J_{SC} of the monoCNTAZ. To better understand the negative effect of the second cyano addition, further characterization is required, and in the next sections, we will gain a deeper understanding of the differences in the photovoltaic parameters (V_{OC}, J_{SC}, and FF) by investigating the morphology, charge recombination dynamics, and CT state of the three polymers.

2.4. Morphology and Fill Factor. To further understand the effect of cyano substitution on molecular ordering of polymers and the morphology of the active layer of BHJ devices, we utilized synchrotron-radiation-based grazing incidence wide-angle X-ray scattering (GIWAXS)[31] to investigate the texture and packing of the polymers in neat films and blends with PCBM (Figures 3 and S4). In the neat polymer films (Figure 3a–c), there are some interesting effects of the cyano substituents. In the case of HTAZ, there is no preferred orientation, as the (010) $\pi-\pi$ stacking peak and (h00) lamella peak are both in the out-of-plane (OOP) direction. With the addition of the first cyano group, i.e., monoCNTAZ, the polymer has a slightly stronger preference toward the face-on orientation, as the (100) and (200) contributions to the in-plane (IP) direction are increased. Similarly, the addition of the second cyano group, i.e., diCNTAZ, has an even stronger preference toward a face-on orientation, as the contribution of the (h00) lamella peaks are increased further in the IP direction. This trend of an increase in cyano substitution leading to an increase in face-on preferential ordering would suggest that the diCNTAZ would have the best performance, as face-on is beneficial for charge transport.[32−37] However, when the polymers are blended with PCBM, the fine difference between polymers quickly vanishes, as all three BHJ blends have a general isotropic ordering. There is, however, a trend with the $\pi-\pi$ stacking distances of the polymers in blends, determined through the OOP (010) peak, getting smaller: 3.98, 3.92, and 3.85 Å for HTAZ, monoCNTAZ, and diCNTAZ blends, respectively. This observation indicates that cyano units on the polymer backbone might strengthen the $\pi-\pi$ stacking within the system. Nevertheless, the coherence lengths of the (010) peaks of the three polymers in BHJ blends are similar to each other (~3 nm), as shown in Table 3, meaning the difference in the polymer crystallinity is minimal.

Since GIWAXS detects only the crystalline part of the samples, we utilized resonant soft X-ray scattering (RSoXS) to inspect the domain information in the polymer:PCBM blends (Figure S5).[38] The long period (related to domain spacing) of the three polymer:PCBM blends is generally similar; specifically, monoCNTAZ blend has smaller domain spacing of ~36 nm than the other two polymer:PCBM blends (~46 nm). However, since the weight ratio of the polymers to PCBM is 1:2 for all samples, the domain sizes of the polymers phase are estimated to be 12 and 15 nm, which are all in the range of the exciton diffusion distance. While this difference

DOI: 10.1021/acsapm.9b00767
ACS Appl. Polym. Mater. 2019, 1, 3313−3322

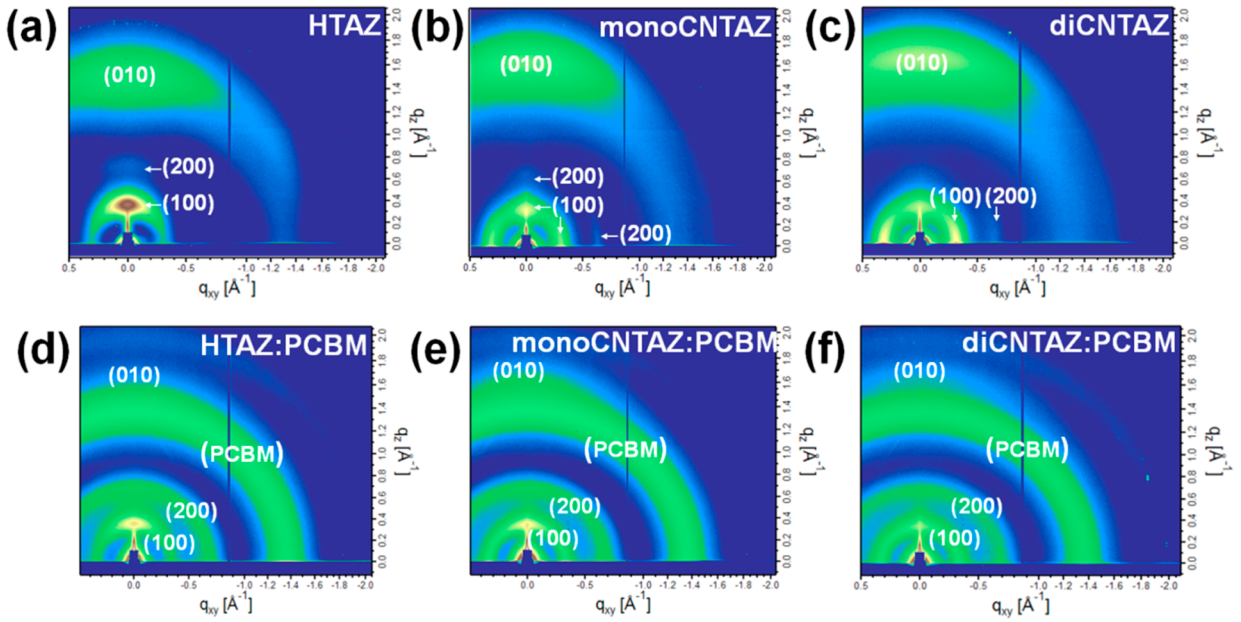

Figure 3. 2D GIWAXS patterns of neat films of (a) HTAZ, (b) monoCNTAZ, and (c) diCNTAZ and blend films of (d) HTAZ:PCBM, (e) monoCNTAZ:PCBM, and (f) diCNTAZ:PCBM.

Table 3. Mobility and Morphological Features of Polymer:PCBM Blends

blend	$\pi-\pi$ stacking distance (Å)	(010) peak coherence length (Å)	long period (nm)	relative domain purity	hole mobility ($cm^2\ V^{-1}\ s^{-1}$)
HTAZ:PCBM	3.98	31.2	45.7	0.73	0.18×10^{-3}
monoCNTAZ:PCBM	3.92	27.8	36.6	1.00	1.08×10^{-3}
diCNTAZ:PCBM	3.85	27.8	48.2	0.88	0.07×10^{-3}

might have some effect on the J_{SC} and EQE, we do not believe this is the dominant cause for the observed difference in the photovoltaic characteristics, as the morphological differences are minor. Furthermore, the domain purity (Table 3) of the monoCNTAZ:PCBM blends is the highest among the three polymer:PCBM blends. The mean-square composition variation, as defined by the integral of the scattering profiles over the length scale probed, is a widely used indicator related to the average domain purity of the OPV blend. The more pure domains of monoCNTAZ:PCBM can help minimize the amount of bimolecular recombination and improve the FF.

Overall, the morphologies of all three polymer:PCBM blends are similar, indicating that cyano substituents on the TAZ units would not strongly affect the overall morphology of the blends. The lower FF of diCNTAZ-based devices stems from a more impure domain, while the higher purity domain of monoCNTAZ-based devices results in the highest FF. Additionally, hole mobilities of the polymer:PCBM blends were also measured and demonstrate a similar trend (Figure S3b and Table S1). Hole mobility, measured through space-charge limited current (SCLC), of the monoCNTAZ:PCBM blend is highest with a value of 1.08×10^{-3} $cm^2/(V{\cdot}s)$, which is much higher than the HTAZ:PCBM blend (0.18×10^{-3} $cm^2/(V{\cdot}s)$) and diCNTAZ:PCBM blend (0.07×10^{-3} $cm^2/(V{\cdot}s)$). These values match the same trend found in the neat polymer blends (Figure S3a and Table S1). In our previous study, we found that hole mobility strongly influences the FF of TAZ-based polymers.[16,39] For the cyano-substituted polymers, the noticeably enhanced hole mobility of monoCNTAZ above the threshold ($\sim 1 \times 10^{-3}$ $cm^2/(V{\cdot}s)$) induces high FF of thick solar cell devices compared to HTAZ and diCTNAZ. Therefore, both the low hole mobility and lower domain purity of diCNTAZ-based devices contributes to the lower J_{SC} and FF. This begins to describe why the second cyano substituent causes a decrease in performance.

2.5. CT State and V_{OC} Loss. V_{OC} values are expected to be enhanced by cyano substitution, as the HOMO energy levels of the polymers are effectively decreased, as demonstrated by the CV data (vide supra). Noticeably enhanced V_{OC} values were achieved by monoCNTAZ and diCNTAZ compared to the nonfunctionalized HTAZ polymer. Moreover, the increase of V_{OC} values from HTAZ to monoCNTAZ (0.19 V) is near 3 times of that from monoCNTAZ to diCNTAZ (0.07 V). The trend of increasing V_{OC} matches the decreasing of HOMO energy levels of the polymers and indicates that the second cyano unit has much less impact than the first cyano unit does, which was also observed by Casey et al.[22] Although the deeper HOMO levels of monoCNTAZ and diCNTAZ explain well the higher V_{OC} values, the V_{OC} is more directly related with the CT state energy (E_{CT}). The CT states more directly affect the V_{OC} of solar cells as illustrated in eq 1,[40] where k is Boltzmann's constant, q is the elementary charge, J_{ph} is the photogenerated current density, J_o is the dark current density, λ is the reorganization energy associated with the CT absorption process, and EQE_{EL} is the electroluminescence external quantum efficiency. We measured the energies of CT states with high sensitive EQE (Figure S6) and fitted the spectra to eq 2,[40] where E is the photon energy, and EQE_{PV} is the photovoltaic EQE. Total energy loss ($E_{opt} - eV_{OC}$) in the device is divided into two parts: (1) from minimum of the optical band gap of the components of the devices to the CT state: ($E_{opt} - E_{CT}$), which acts as the driving force for the

DOI: 10.1021/acsapm.9b00767
ACS Appl. Polym. Mater. 2019, 1, 3313−3322

exciton splitting; and (2) from the CT state to V_{OC}: ($E_{CT} - eV_{OC}$), which originates from the nongeminate recombination.[41]

$$V_{oc} = \frac{kT}{q}\ln\left(\frac{J_{ph}}{J_0} + 1\right) = \frac{E_{CT}}{q} + \frac{kT}{q}\ln\left(\frac{J_{sc}h^3c^2}{fq2\pi(E_{CT} - \lambda)}\right) + \frac{kT}{q}\ln(EQE_{EL}) \quad (1)$$

$$EQE_{PV}(E) = \frac{f}{E\sqrt{4\pi\lambda kT}}\exp\left(\frac{-(E_{CT} + \lambda - E)^2}{4\lambda kT}\right) \quad (2)$$

The energies of the CT states and the V_{OC} losses of devices are summarized in Table 4. The loss from the CT state to the V_{OC} (~0.62 eV) is similar for all the three polymer-based devices, indicating the nongeminate recombination caused V_{OC} loss is similar for the three polymers. However, there is a noticeable difference in the loss from the minimum band gap to the CT state: the driving force for the exciton splitting gets reduced with the cyano substitution. For the diCNTAZ, the CT state energy is close to the minimum band gap, and the driving force is extremely low. Though this high-lying CT state is beneficial for the high V_{OC} obtained, the low driving force in the diCNTAZ-based devices may harm the exciton splitting and hole transport from the PCBM to diCNTAZ, especially if there is energy transfer from diCNTAZ to PCBM, which will increase the geminate recombination in the device and decrease the J_{SC} of diCNTAZ-based devices.[42,43]

Since we have already demonstrated the negative effect on hole mobility with the addition of the second cyano group, exciton splitting was explored next. To further understand the reasons of the different J_{SC} values of monoCNTAZ and diCNTAZ, quenching of excitons in polymer:PCBM blend was investigated by photoluminescence (PL) (Figure S7). Comparably high PL quenching efficiency was observed in both cases for diCNTAZ:PCBM (96%) and monoCNTAZ:PCBM (98%), which suggests that excitons should be effectively split; however, this high PL quench does not rule out geminate recombination, as mentioned above, because energy transfer from diCNTAZ to PCBM is possible. Therefore, while the addition of further cyano groups can allow for a high V_{OC} and decrease V_{OC} loss, the decrease in exciton driving force and decreased hole mobility results in a lower J_{SC}. As the improvement in V_{OC} is minor with the addition of the second cyano group, the optimized functionalization of a single cyano group (i.e., monoCNTAZ) demonstrates the ideal balance between improvements of photovoltaic parameters.

2.6. Charge Recombination Dynamics. To further investigate the influence of cyano substitutions on device characteristics, transient photocurrent (TPC) and transient photovoltage (TPV) measurements were undertaken to determine the lifetime, density, and recombination dynamics in the active layer,[29,44,45] using fresh devices with the ITO/PEDOT:PSS/polymer:PCBM/PFN/Al device architecture. First, we measured charge carrier density as a function of V_{OC} for the devices (Figure 4a). Variations of V_{OC} between 0.60−0.76 V for the HTAZ:PCBM device, 0.69−0.93 V for monoCNTAZ:PCBM, and 0.76−1.03 V for the diCNTAZ:PCBM device were achieved by adjusting the intensity light between 2−100 mW/cm^2, a method previously outlined in literature.[46] The $n(V_{OC})$ characteristics visualize the bulk quasi-Fermi level splitting in the photoactive layer at different illumination intensities, thus representing how far away the active layer is from equilibrium under operation conditions.[47,48] At a representative charge density range of $1-2 \times 10^{-16}$ cm^{-3}, the quasi-Fermi level splitting is largest for the diCNTAZ:PCBM device, consistent with the largest measured open-circuit voltage. It is worth noting that the measured charge density in all devices increases exponentially as a function of V_{OC}, following a relationship $n = n_0e^{\gamma V_{OC}}$, where n_0 is the charge density in the dark, and γ is the slope of the $\ln(n) \sim V_{OC}$ curves (Figure 4a). A clear trend in the slope is observed with the three polymers: as the amount of cyano groups on the polymer increases, the slope decreases. While diCNTAZ has the lowest slope (γ), the highest $n(V_{OC})$ value results in an increase in the J_{loss}, as described in eq 3. This can also help describe the lower J_{SC} value of diCNTAZ compared to monoCNTAZ.

Next, the measured charge carrier lifetime in the devices as a function of V_{OC} is depicted in Figure 4b. For all of the devices, the lifetime decreases exponentially as a function of V_{OC} via $\tau_{\Delta n} = \tau_{\Delta n_0}e^{-\beta V_{OC}}$, where $\tau_{\Delta n_0}$ is the carrier lifetime in the dark, and β is the decay constant. Because the devices show a decreasing lifetime as the charge carrier density increases, following a power law dependence with charge density, nongeminate recombination is likely to be the dominant recombination pathway for loss in the device. Therefore, the loss current can be quantified via eq 3,[29] where $k(n)$ is the nongeminate recombination rate coefficient and is given by eq 4, e is the elementary charge, d is the photoactive layer thickness, $n(V_{OC})$ is the measured charge carrier density (shown in Figure 4a), and $\tau(V_{OC})$is the measured carrier lifetime (shown in Figure 4b) obtained under different illumination intensities.

$$J_{loss} = edk(n)n^2 = ed\frac{n(V_{OC})}{\tau(V_{OC})} \quad (3)$$

$$k(n) = \frac{1}{\left(1 + \frac{\beta}{\gamma}\right)n\tau_{\Delta n}} \quad (4)$$

The measured $k(n)$ for all devices is depicted in Figure 4c. While it is clear that the diCNTAZ:PCBM device shows the lowest $k(n)$ at high charge carrier densities among all three investigated BHJ devices, the dependence on carrier density for the diCNTAZ:PCBM device is also larger (i.e., larger slope—small changes in charge carrier density result in higher recombination rate coefficients). On the other hand, while the monoCNTAZ:PCBM device also shows a reduced nongeminate recombination rate coefficient compared to the HTAZ:PCBM device at low charge densities, it is only at higher charge carrier densities that the monoCNTAZ:PCBM

Table 4. CT State Energy and the V_{oc} Loss of the Devices

polymer	V_{OC} (V)	E_{opt}[a] (eV)	E_{CT} (eV)	$E_{CT} - eV_{OC}$ (eV)	$E_{opt} - E_{CT}$ (eV)	total loss (eV)
HTAZ	0.74	1.66	1.36	0.62	0.30	0.92
monoCNTAZ	0.93	1.66	1.56	0.63	0.10	0.73
diCNTAZ	1.00	1.66	1.61	0.61	0.05	0.66

[a]Smaller optical bandgap (E_{opt}) of the two components, which is PCBM in these cases.

DOI: 10.1021/acsapm.9b00767
ACS Appl. Polym. Mater. 2019, 1, 3313−3322

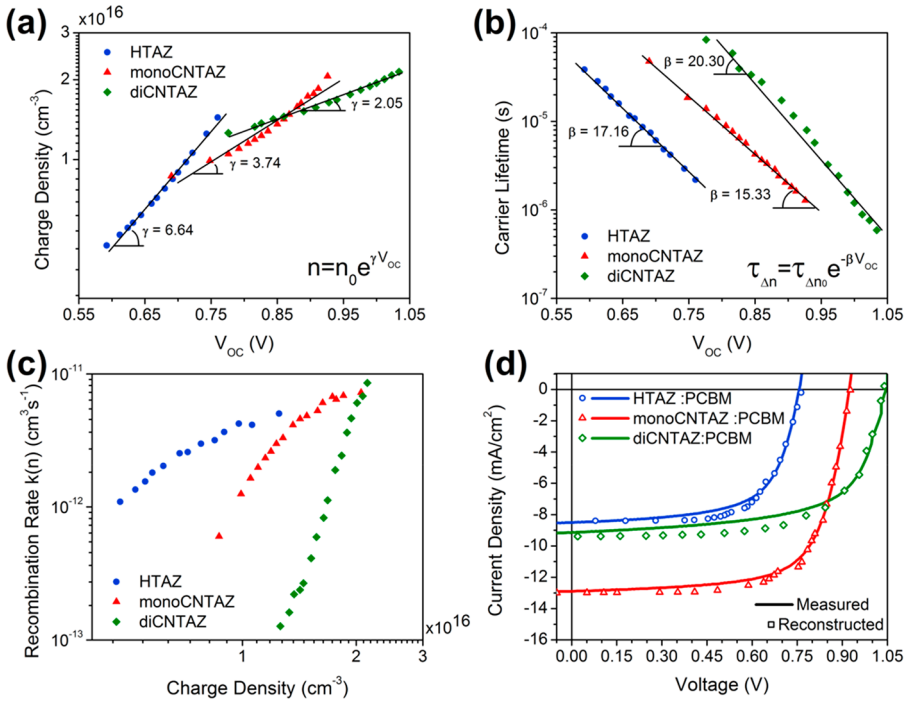

Figure 4. (a) Measured charge carrier density (n) as a function of V_{OC} and (b) measured charge carrier lifetime as a function of V_{OC}. Solid lines represent the fit to each equation (shown on the graph), with the slopes shown next to each fit. (c) The calculated nongeminate recombination rate coefficient as a function of charge carrier density. (d) Reconstructed $J-V$ characteristics (open symbols) vs measured $J-V$ characteristics (solid line), assuming that only nongeminate recombination contributes to losses.

device has a lower recombination rate coefficient than the diCNTAZ:PCBM device. As a result of reduced nongeminate recombination losses, the diCNTAZ:PCBM device and monoCNTAZ:PCBM device can afford higher charge accumulation and therefore lead to a larger quasi-Fermi level splitting than the HTAZ:PCBM device, accounting for high V_{OC} values for the former two types of devices. However, as the charge carrier density increases, diCNTAZ:PCBM devices have a recombination rate that surpasses those rates of the other two blends, which can result in detrimental device performance. The $\tau_{\Delta n_0}$, the charge carrier lifetime in the dark, for the diCNTAZ:PCBM device (904 s) is substantially larger than the monoCNTAZ:PCBM device (2 s) and the HTAZ:PCBM device (1 s), which can result in the larger accumulation of charges, and while this boosts V_{OC}, the diCNTAZ:PCBM device has an increasingly higher recombination rate coefficient with charge carrier density. This is also consistent the significantly lower mobility values measured for the diCNTAZ:PCBM device. Therefore, while the addition of the second cyano group allows for higher charge carrier density and lifetimes, it also results in increased recombination and lower J_{SC}. In the case of the monoCNTAZ:PCBM device, the balance between charge carrier density and lifetime results in the improved performance and less recombination.

To demonstrate the validity of this approach, the current density can be predicted at the various V_{OC} values, and a $J-V$ curve can be simulated.[49] As shown in Figure 4d, the reconstructed and the measured $J-V$ curves coincide well with each other, verifying that nongeminate recombination is in fact the dominating loss pathway for these devices.[50] Furthermore, in case that nongeminate recombination of charge carriers is negligible at short-circuit conditions, the open-circuit voltage under one sun illumination can be calculated and thus enables a quantitative assessment of impact of changes in the energetics and recombination rate on V_{OC}. The open-circuit voltages under AM 1.5G illumination predicted by eq 5 are 0.796 V for the HTAZ:PCBM device, 0.932 V for the monoCNTAZ:PCBM device, and 1.060 V for the diCNTAZ:PCBM device, in excellent agreement with the measured values (0.75, 0.92, and 1.05 V, respectively), confirming the validity of transient optoelectronic analyses.

$$V_{OC} = \frac{1}{\beta + \gamma} \ln\left(\frac{J_{SC}\tau_{\Delta n_0}\left(1 + \frac{\beta}{\gamma}\right)}{edn_0}\right) \quad (5)$$

These results and analyses show that the cyano groups play a very important role in the charge recombination dynamics. Adding cyano substituents can boost the V_{OC} from the increase in charge carrier density and lifetime; however, in the case of diCNTAZ, this also results in a larger dependence of the charge carrier density on recombination rate coefficients. The best device of monoCNTAZ:PCBM shows the higher J_{SC} and FF mainly due to its higher charge mobilities and the balance between recombination kinetics and charge extraction in the devices.[51]

3. CONCLUSION

In this study, we gradually increased the amount of cyano substituent on conjugated polymers and systematically studied the effect of cyano substitution on properties of polymers. The strong electron-withdrawing cyano unit can effectively tune the energy levels and band gaps; with deepened energy levels, the cyano-substituted polymers achieve high V_{OC}. The cyano substituent also proves efficient in decreasing optical band gaps and shifting the absorption of polymers to long wavelength,

DOI: 10.1021/acsapm.9b00767
ACS Appl. Polym. Mater. 2019, 1, 3313−3322

which benefits the J_{SC} of solar cells. Moreover, the cyano unit also decreases the $\pi-\pi$ stacking distance and improves the charge transport properties of monoCNTAZ. With all the three parameters (V_{OC}, J_{SC}, and FF) improved, monoCNTAZ achieved a high PCE of 8.6% with PCBM as the electron acceptor. However, further addition of cyano groups shows degradation in the device performance, driven by a decrease in the mobility and purity of domains, along with an increase in charge recombination. This study proves the benefit of incorporating the cyano unit in conjugated polymers to improve properties of polymers and provides guidelines to optimize structure of polymers.

■ ASSOCIATED CONTENT

Supporting Information

The Supporting Information is available free of charge on the ACS Publications website at DOI: 10.1021/acsapm.9b00767.

Synthetic details for monomers and polymer, ^{1}H and ^{13}C NMR spectra, characterization methods and device fabrication, PL and CT state measurements, GIWAXS, RSoXS profiles, and line fitting for GIWAXS blends (PDF)

■ AUTHOR INFORMATION

Corresponding Author

*E-mail: wyou@unc.edu.

ORCID

Jeromy James Rech: 0000-0001-7963-9357
Liang Yan: 0000-0003-4122-7466
Hongbin Wu: 0000-0003-2770-6188
Wei You: 0000-0003-0354-1948

Notes

The authors declare no competing financial interest.

■ ACKNOWLEDGMENTS

Q.Q.Z., J.J.R, L.Y., Z.X.P., H.A., and W.Y. were supported by NSF CBET-1639429; Q.B.L. and H.B.W. were supported by the National Nature Science Foundation of China (No. 51521002). We want to thank Wesley Swords and Professor Gerald Meyer for assistance with PL measurements. In addition, we want to thank Prof. David Haddleton and Sam Lawton (University of Warwick) for HT-GPC measurements and the UNC Department of Chemistry Mass Spectrometry Core Laboratory for mass spectrometry measurement. GIWAXS/RSoXS measurements and analysis were supported by NSF CBET-1639429. GIWAXS/RSoXS data was collected at beamline 7.3.3, at the Advanced Light Source in Berkeley National Lab, supported by the US Department of Energy (No. DE-AC02-05CH11231). The authors would also like to thank Maruti Hegde and Professor Theo Dingemans for help with the TGA and DSC measurements.

■ REFERENCES

(1) Kippelen, B.; Brédas, J.-L. Organic Photovoltaics. *Energy Environ. Sci.* **2009**, *2*, 251.

(2) Hou, J.; Inganäs, O.; Friend, R. H.; Gao, F. Organic Solar Cells Based on Non-Fullerene Acceptors. *Nat. Mater.* **2018**, *17*, 119−128.

(3) Wang, G.; Melkonyan, F. S.; Facchetti, A.; Marks, T. J. All-Polymer Solar Cells: Recent Progress, Challenges, and Prospects. *Angew. Chem., Int. Ed.* **2019**, *58*, 4129−4142.

(4) Li, H.; Lu, K.; Wei, Z. Polymer/Small Molecule/Fullerene Based Ternary Solar Cells. *Adv. Energy Mater.* **2017**, *7*, 1602540.

(5) Ma, Y.; Kang, Z.; Zheng, Q. Recent Advances in Wide Bandgap Semiconducting Polymers for Polymer Solar Cells. *J. Mater. Chem. A* **2017**, *5*, 1860−1872.

(6) Zhou, H.; Yang, L.; You, W. Rational Design of High Performance Conjugated Polymers for Organic Solar Cells. *Macromolecules* **2012**, *45*, 607−632.

(7) Xiao, S.; Zhang, Q.; You, W. Molecular Engineering of Conjugated Polymers for Solar Cells: An Updated Report. *Adv. Mater.* **2017**, *29*, 1601391.

(8) Bauer, N.; Zhang, Q.; Zhu, J.; Peng, Z.; Yan, L.; Zhu, C.; Ade, H.; Zhan, X.; You, W. Donor Polymer Fluorination Doubles the Efficiency in Non-Fullerene Organic Photovoltaics. *J. Mater. Chem. A* **2017**, *5*, 22536−22541.

(9) Jo, J. W.; Bae, S.; Liu, F.; Russell, T. P.; Jo, W. H. Comparison of Two D−A Type Polymers with Each Being Fluorinated on D and A Unit for High Performance Solar Cells. *Adv. Funct. Mater.* **2015**, *25*, 120−125.

(10) Ibraikulov, O. A.; Ngov, C.; Chavez, P.; Bulut, I.; Heinrich, B.; Boyron, O.; Gerasimov, K. L.; Ivanov, D. A.; Swaraj, S.; Mery, S.; Leclerc, N.; Leveque, P.; Heiser, T. Face-on Orientation of Fluorinated Polymers Conveyed by Long Alkyl Chains: A Prerequisite for High Photovoltaic Performances. *J. Mater. Chem. A* **2018**, *6*, 12038.

(11) Zhang, S.; Qin, Y.; Uddin, M. A.; Jang, B.; Zhao, W.; Liu, D.; Woo, H. Y.; Hou, J. A Fluorinated Polythiophene Derivative with Stabilized Backbone Conformation for Highly Efficient Fullerene and Non-Fullerene Polymer Solar Cells. *Macromolecules* **2016**, *49*, 2993−3000.

(12) Zhang, Z.-G.; Li, Y. Side-Chain Engineering of High-Efficiency Conjugated Polymer Photovoltaic Materials. *Sci. China: Chem.* **2015**, *58*, 192−209.

(13) Zhang, Q.; Kelly, M. A.; Bauer, N.; You, W. The Curious Case of Fluorination of Conjugated Polymers for Solar Cells. *Acc. Chem. Res.* **2017**, *50*, 2401−2409.

(14) Meyer, F. Fluorinated Conjugated Polymers in Organic Bulk Heterojunction Photovoltaic Solar Cells. *Prog. Polym. Sci.* **2015**, *47*, 70−91.

(15) Leclerc, N.; Chávez, P.; Ibraikulov, O.; Heiser, T.; Lévêque, P. Impact of Backbone Fluorination on π-Conjugated Polymers in Organic Photovoltaic Devices: A Review. *Polymers (Basel, Switz.)* **2016**, *8*, 11.

(16) Zhang, Q.; Yan, L.; Jiao, X.; Peng, Z.; Liu, S.; Rech, J. J.; Klump, E.; Ade, H.; So, F.; You, W. Fluorinated Thiophene Units Improve Photovoltaic Device Performance of Donor−Acceptor Copolymers. *Chem. Mater.* **2017**, *29*, 5990−6002.

(17) Kelly, M. A.; Zhang, Q.; Peng, Z.; Noman, V.; Zhu, C.; Ade, H.; You, W. The Finale of a Trilogy: Comparing Terpolymers and Ternary Blends with Structurally Similar Backbones for Use in Organic Bulk Heterojunction Solar Cells. *J. Mater. Chem. A* **2018**, *6*, 19190−19200.

(18) Qiu, M.; Brandt, R. G.; Niu, Y.; Bao, X.; Yu, D.; Wang, N.; Han, L.; Yu, L.; Xia, S.; Yang, R. Theoretical Study on the Rational Design of Cyano-Substituted P3HT Materials for OSCs: Substitution Effect on the Improvement of Photovoltaic Performance. *J. Phys. Chem. C* **2015**, *119*, 8501−8511.

(19) Cha, H.; Kim, H. N.; An, T. K.; Kang, M. S.; Kwon, S.-K.; Kim, Y.-H.; Park, C. E. Effects of Cyano-Substituents on the Molecular Packing Structures of Conjugated Polymers for Bulk-Heterojunction Solar Cells. *ACS Appl. Mater. Interfaces* **2014**, *6*, 15774−15782.

(20) Kim, H. G.; Kim, M.; Clement, J. A.; Lee, J.; Shin, J.; Hwang, H.; Sin, D. H.; Cho, K. Energy Level Engineering of Donor Polymers via Inductive and Resonance Effects for Polymer Solar Cells: Effects of Cyano and Alkoxy Substituents. *Chem. Mater.* **2015**, *27*, 6858−6868.

(21) Li, W.; Yan, L.; Zhou, H.; You, W. A General Approach toward Electron Deficient Triazole Units to Construct Conjugated Polymers for Solar Cells. *Chem. Mater.* **2015**, *27*, 6470−6476.

(22) Casey, A.; Dimitrov, S. D.; Shakya-Tuladhar, P.; Fei, Z.; Nguyen, M.; Han, Y.; Anthopoulos, T. D.; Durrant, J. R.; Heeney, M.

DOI: 10.1021/acsapm.9b00767
ACS Appl. Polym. Mater. 2019, 1, 3313−3322

Effect of Systematically Tuning Conjugated Donor Polymer Lowest Unoccupied Molecular Orbital Levels via Cyano Substitution on Organic Photovoltaic Device Performance. *Chem. Mater.* **2016**, *28*, 5110−5120.
(23) Casey, A.; Green, J. P.; Shakya Tuladhar, P.; Kirkus, M.; Han, Y.; Anthopoulos, T. D.; Heeney, M. Cyano Substituted Benzotriazole Based Polymers for Use in Organic Solar Cells. *J. Mater. Chem. A* **2017**, *5*, 6465−6470.
(24) Price, S. C.; Stuart, A. C.; Yang, L.; Zhou, H.; You, W. Fluorine Substituted Conjugated Polymer of Medium Band Gap Yields 7% Efficiency in Polymer−Fullerene Solar Cells. *J. Am. Chem. Soc.* **2011**, *133*, 4625−4631.
(25) Wudarczyk, J.; Papamokos, G.; Margaritis, V.; Schollmeyer, D.; Hinkel, F.; Baumgarten, M.; Floudas, G.; Müllen, K. Hexasubstituted Benzenes with Ultrastrong Dipole Moments. *Angew. Chem., Int. Ed.* **2016**, *55*, 3220−3223.
(26) Li, W.; Yang, L.; Tumbleston, J. R.; Yan, L.; Ade, H.; You, W. Controlling Molecular Weight of a High Efficiency Donor-Acceptor Conjugated Polymer and Understanding Its Significant Impact on Photovoltaic Properties. *Adv. Mater.* **2014**, *26*, 4456−4462.
(27) Kelly, M. A.; Roland, S.; Zhang, Q.; Lee, Y.; Kabius, B.; Wang, Q.; Gomez, E. D.; Neher, D.; You, W. Incorporating Fluorine Substitution into Conjugated Polymers for Solar Cells: Three Different Means, Same Results. *J. Phys. Chem. C* **2017**, *121*, 2059−2068.
(28) Pattanasattayavong, P.; Yaacobi-Gross, N.; Zhao, K.; Ndjawa, G. O. N.; Li, J.; Yan, F.; O'Regan, B. C.; Amassian, A.; Anthopoulos, T. D. Hole-Transporting Transistors and Circuits Based on the Transparent Inorganic Semiconductor Copper(I) Thiocyanate (CuSCN) Processed from Solution at Room Temperature. *Adv. Mater.* **2013**, *25*, 1504−1509.
(29) Hamilton, R.; Shuttle, C. G.; O'Regan, B.; Hammant, T. C.; Nelson, J.; Durrant, J. R. Recombination in Annealed and Non-annealed Polythiophene/Fullerene Solar Cells: Transient Photovoltage Studies versus Numerical Modeling. *J. Phys. Chem. Lett.* **2010**, *1*, 1432−1436.
(30) He, Z.; Zhong, C.; Huang, X.; Wong, W.-Y.; Wu, H.; Chen, L.; Su, S.; Cao, Y. Simultaneous Enhancement of Open-Circuit Voltage, Short-Circuit Current Density, and Fill Factor in Polymer Solar Cells. *Adv. Mater.* **2011**, *23*, 4636−4643.
(31) Hexemer, A.; Bras, W.; Glossinger, J.; Schaible, E.; Gann, E.; Kirian, R.; MacDowell, A.; Church, M.; Rude, B.; Padmore, H. A SAXS/WAXS/GISAXS Beamline with Multilayer Monochromator. *J. Phys. Conf. Ser.* **2010**, *247*, No. 012007.
(32) Li, S.; Ye, L.; Zhao, W.; Liu, X.; Zhu, J.; Ade, H.; Hou, J. Design of a New Small-Molecule Electron Acceptor Enables Efficient Polymer Solar Cells with High Fill Factor. *Adv. Mater.* **2017**, *29*, 1704051.
(33) Yao, H.; Li, Y.; Hu, H.; Chow, P. C. Y.; Chen, S.; Zhao, J.; Li, Z.; Carpenter, J. H.; Lai, J. Y. L.; Yang, G.; Liu, Y.; Lin, H.; Ade, H.; Yan, H. A Facile Method to Fine-Tune Polymer Aggregation Properties and Blend Morphology of Polymer Solar Cells Using Donor Polymers with Randomly Distributed Alkyl Chains. *Adv. Energy Mater.* **2018**, *8*, 1701895.
(34) Duan, C.; Gao, K.; van Franeker, J. J.; Liu, F.; Wienk, M. M.; Janssen, R. A. J. Toward Practical Useful Polymers for Highly Efficient Solar Cells via a Random Copolymer Approach. *J. Am. Chem. Soc.* **2016**, *138*, 10782−10785.
(35) Mai, J.; Xiao, Y.; Zhou, G.; Wang, J.; Zhu, J.; Zhao, N.; Zhan, X.; Lu, X. Hidden Structure Ordering Along Backbone of Fused-Ring Electron Acceptors Enhanced by Ternary Bulk Heterojunction. *Adv. Mater.* **2018**, *30*, 1802888.
(36) Su, Y.-W.; Lin, Y.-C.; Wei, K.-H. Evolving Molecular Architectures of Donor−Acceptor Conjugated Polymers for Photovoltaic Applications: From One-Dimensional to Branched to Two-Dimensional Structures. *J. Mater. Chem. A* **2017**, *5*, 24051−24075.
(37) Zhang, H.; Wang, X.; Yang, L.; Zhang, S.; Zhang, Y.; He, C.; Ma, W.; Hou, J. Improved Domain Size and Purity Enables Efficient All-Small-Molecule Ternary Solar Cells. *Adv. Mater.* **2017**, *29*, 1703777.
(38) Rivnay, J.; Mannsfeld, S. C. B.; Miller, C. E.; Salleo, A.; Toney, M. F. Quantitative Determination of Organic Semiconductor Microstructure from the Molecular to Device Scale. *Chem. Rev.* **2012**, *112*, 5488−5519.
(39) Li, W.; Albrecht, S.; Yang, L.; Roland, S.; Tumbleston, J. R.; McAfee, T.; Yan, L.; Kelly, M. A.; Ade, H.; Neher, D.; You, W. Mobility-Controlled Performance of Thick Solar Cells Based on Fluorinated Copolymers. *J. Am. Chem. Soc.* **2014**, *136*, 15566−15576.
(40) Vandewal, K.; Tvingstedt, K.; Gadisa, A.; Inganäs, O.; Manca, J. V. Relating the Open-Circuit Voltage to Interface Molecular Properties of Donor:Acceptor Bulk Heterojunction Solar Cells. *Phys. Rev. B: Condens. Matter Mater. Phys.* **2010**, *81*, 125204.
(41) Faist, M. A.; Kirchartz, T.; Gong, W.; Ashraf, R. S.; McCulloch, I.; de Mello, J. C.; Ekins-Daukes, N. J.; Bradley, D. D. C.; Nelson, J. Competition between the Charge Transfer State and the Singlet States of Donor or Acceptor Limiting the Efficiency in Polymer:-Fullerene Solar Cells. *J. Am. Chem. Soc.* **2012**, *134*, 685−692.
(42) Hoke, E. T.; Vandewal, K.; Bartelt, J. A.; Mateker, W. R.; Douglas, J. D.; Noriega, R.; Graham, K. R.; Fréchet, J. M. J.; Salleo, A.; McGehee, M. D. Recombination in Polymer:Fullerene Solar Cells with Open-Circuit Voltages Approaching and Exceeding 1.0 V. *Adv. Energy Mater.* **2013**, *3*, 220−230.
(43) Roland, S.; Yan, L.; Zhang, Q.; Jiao, X.; Hunt, A.; Ghasemi, M.; Ade, H.; You, W.; Neher, D. Charge Generation and Mobility-Limited Performance of Bulk Heterojunction Solar Cells with a Higher Adduct Fullerene. *J. Phys. Chem. C* **2017**, *121*, 10305−10316.
(44) Shuttle, C. G.; O'Regan, B.; Ballantyne, A. M.; Nelson, J.; Bradley, D. D. C.; de Mello, J.; Durrant, J. R. Experimental Determination of the Rate Law for Charge Carrier Decay in a Polythiophene: Fullerene Solar Cell. *Appl. Phys. Lett.* **2008**, *92*, No. 093311.
(45) Barnes, P. R. F.; Miettunen, K.; Li, X.; Anderson, A. Y.; Bessho, T.; Gratzel, M.; O'Regan, B. C. Interpretation of Optoelectronic Transient and Charge Extraction Measurements in Dye-Sensitized Solar Cells. *Adv. Mater.* **2013**, *25*, 1881−1922.
(46) Credgington, D.; Hamilton, R.; Atienzar, P.; Nelson, J.; Durrant, J. R. Non-Geminate Recombination as the Primary Determinant of Open-Circuit Voltage in Polythiophene:Fullerene Blend Solar Cells: An Analysis of the Influence of Device Processing Conditions. *Adv. Funct. Mater.* **2011**, *21*, 2744−2753.
(47) Shuttle, C. G.; Hamilton, R.; Nelson, J.; O'Regan, B. C.; Durrant, J. R. Measurement of Charge-Density Dependence of Carrier Mobility in an Organic Semiconductor Blend. *Adv. Funct. Mater.* **2010**, *20*, 698−702.
(48) Shuttle, C. G.; Maurano, A.; Hamilton, R.; O'Regan, B.; de Mello, J. C.; Durrant, J. R. Charge Extraction Analysis of Charge Carrier Densities in a Polythiophene/Fullerene Solar Cell: Analysis of the Origin of the Device Dark Current. *Appl. Phys. Lett.* **2008**, *93*, 183501.
(49) Shuttle, C. G.; Hamilton, R.; O'Regan, B. C.; Nelson, J.; Durrant, J. R. Charge-Density-Based Analysis of the Current-Voltage Response of Polythiophene/Fullerene Photovoltaic Devices. *Proc. Natl. Acad. Sci. U. S. A.* **2010**, *107*, 16448−16452.
(50) Yan, J.; Luo, G.; Xiao, B.; Wu, H.; He, Z.; Cao, Y. Origin of High Fill Factor in Polymer Solar Cells from Semiconducting Polymer with Moderate Charge Carrier Mobility. *Org. Electron.* **2015**, *24*, 125−130.
(51) Bartesaghi, D.; Pérez, I. D. C.; Kniepert, J.; Roland, S.; Turbiez, M.; Neher, D.; Koster, L. J. A. Competition between Recombination and Extraction of Free Charges Determines the Fill Factor of Organic Solar Cells. *Nat. Commun.* **2015**, *6*, 7083.

DOI: 10.1021/acsapm.9b00767
ACS Appl. Polym. Mater. 2019, 1, 3313−3322